Numerical investigations on THM coupled process during water flooding with multiple well patterns under non-isothermal two phase flow

Yuhao Liu
Department of Geotechnical Engineering, College of Civil Engineering, Tongji University, Shanghai, China

Fengshou Zhang
Department of Geotechnical Engineering, College of Civil Engineering, Tongji University, Shanghai, China

Dingwei Weng
Research Institute of Petroleum Exploration & Development, PetroChina, Beijing, China

Hongbo Liang
Research Institute of Petroleum Exploration & Development, PetroChina, Beijing, China

Chunming He
Research Institute of Petroleum Exploration & Development, PetroChina, Beijing, China

ABSTRACT: A three-dimensional numerical model of non-isothermal two-phase flow in the deformable porous medium during water flooding is described in this paper. Based on the thermal-hydro-mechanical (THM) coupling theory, governing equations of oil-water two-phase flow are integrated additionally and implemented into the open-source finite element framework OpenGeoSys. Temperature-dependent fluid viscosity and fluid density, along with strain-dependent reservoir permeability are also considered. With different well patterns, stress and pore pressure distribution, heat transfer and the flow of injected water in the reservoir during ten years of injection are simulated. According to the numerical results, high temperature can promote fluid flow to improve the treatment performance. Cold water injection causes the normal stress reduction by introducing significant thermal stress. Spatial variation of stress, pore pressure and injected water saturation are affected by different well pattern scenarios. This finding has important consequences in the field operation of water flooding under the environment of large reservoir depth and high temperature.

Keywords: Water flooding, THM coupling, Two phase flow, Multiple well patterns, OpenGeoSys.

1 INTRODUTION

Water flooding is a widely used petroleum engineering technique for enhanced oil recovery. In a typical water flooding scenario, several horizontal or vertical wells are arranged to form a certain well pattern containing injection wells and production wells. Continuous pumping of water over months or years will displace the oil and drive it to the nearby production wells. Numerical simulation can compensate for the limitation of experimental researches about water flooding for some detailed investigations, such as macroscopic reservoir production prediction and design optimization(Zhai et al. 2022 and Zhang et al. 2022), along with the microscopic fluid flow behavior in the media at pore-scale (Akai et al. 2020 and Patel et al. 2019). Water flooding under the complex environment during a long-term pumping process is also an important numerical issue but there are still inadequate researches (Douglas, Jr. et al. 1997; Zhang et al. 2016; Zheng et al. 2021). In the current studies, significant thermal effect caused by large buried depth is neglected and numerical modeling of

multiple wells in the field at engineering scale is lacking. Therefore, in this paper we develop a three dimensional fully coupled THM model of different multi-well working scenarios, integrated with two-phase flow. Fluid viscosity and density are temperature-dependent and reservoir permeability is strain-dependent. The mathematical model is executed in the open-source finite element framework OpenGeoSys (Kolditz et al. 2012). A multi-well water flooding model in the fractured reservoir based on Changqing oil field in the northwest China is considered with three-spot, five-spot and seven-spot well patterns. During 10 years of injection and production process, the geomechanical responses of the reservoir are analyzed. Comparison of isothermal and non-isothermal cases is conducted to illustrate the thermal stress around the wellbore and thermal promotion in fluid flow. Different well patterns are also applied to obtain the spatial variation of the geomechanical responses in the reservoir. The work provides a deep understanding of water flooding under the environment of large reservoir depth and high temperature.

2 METHODS AND RESULTS

2.1 Mathematical framework

Based on the THM coupling theory (Parisio et al. 2019), water-oil mixture flow is considered. The mass balance equations for water component and oil component are:

$$n\rho_w \frac{\partial S_w}{\partial \rho_c}\dot{\rho}_c + \nabla \cdot \left[\rho_w \frac{\boldsymbol{k}k_{rw}}{\mu_w}(-\nabla p_{oil} + \nabla p_c + \rho_w \boldsymbol{g})\right] = Q_w \tag{1}$$

$$\begin{aligned} &-n\rho_{oil}\frac{\partial S_w}{\partial p_c}\dot{p}_c + n(1-S_w)\left(\frac{\partial \rho_{oil}}{\partial p_{oil}}\dot{p}_{oil} + \frac{\partial \rho_{oil}}{\partial p_c}\dot{p}_c\right) \\ &+\nabla \cdot \left[\rho_{oil}\frac{\boldsymbol{k}k_{roil}}{\mu_{oil}}(-\nabla p_{oil} + \rho_w \boldsymbol{g})\right] = Q_{oil} \end{aligned} \tag{2}$$

where van Genuchten model (Genuchten 1980) is applied to calculate saturation and relative permeability:

$$S(p_c) = \begin{cases} S_{max}^w & p_c \le 0 \\ \left(\left(\frac{p_c}{p_b}\right)^{\frac{1}{1-m}} + 1\right)^{-m}(S_{max}^w - S_r^w) + S_r^w & p_c > 0 \end{cases}, \quad p_b = \frac{\rho_w g}{\alpha} \tag{3}$$

$$\begin{aligned} &k_{rw} = (S_e)^{\frac{1}{2}}\left(1 - \left(1 - S_e^{\frac{1}{m}}\right)^m\right)^2, \qquad k_{roil} = (1-S_e)^{\frac{1}{2}}\left(1 - S_e^{\frac{1}{m}}\right)^{2m} \\ &S_e = \frac{S^w - S_r^w}{S_{max}^w - S_r^w} \end{aligned} \tag{4}$$

where the maximum and residual saturations of water in our model are 0.85 and 0.19. In addition, temperature-dependent fluid density and viscosity and strain-dependent reservoir permeability from Magri et al. (2017) and Xu et al. (2013) are given in Eq. (5) to Eq. (7):

$$\rho(T) = 1000 \times (1 - 0.00059 \times (T - 293.15)) \tag{5}$$

$$\mu(T) = 0.001 \times e^{-0.0161(T-293.15)} \tag{6}$$

$$\boldsymbol{k} = f(\epsilon_v)e^{b_1\bar{\epsilon}^p}\boldsymbol{k_0}, \qquad f(\epsilon_v) = \begin{cases} 10^{b_2\epsilon_v} & \epsilon_v \le 0 \\ 10^{b_3\epsilon_v} & \epsilon_v > 0 \end{cases} \tag{7}$$

2.2 *Model description*

Figure 1 illustrates the setup of the numerical models. Three kinds of well patterns, i.e., three-spot, five-spot and seven-spot, are applied and the model is constructed in the 600 m×400 m×20 m schematic of reservoir. The initial temperature of reservoir is 71.63 ℃ and the initial pore pressure is 15.8 MPa. All boundaries are closed to fluid flow and constrained in normal displacement directions. To represent the state of fractured reservoir, permeability and porosity are defined as exponential distribution with the same functional shape in Figure 2. All other constant parameters are listed in Table 1. Cold water is injected from the surrounding injection wells at a rate of 6×10^{-5} m^3/s for a total of 10 years of exploitation and drives oil to the central production well with a constant producing pressure of 14.8 MPa. The initial stress field (σ_H, σ_h, σ_v) in the reservoir is 49.01 MPa, 43.57 MPa and 54.46 MPa and the initial water-saturation is 42.78%.

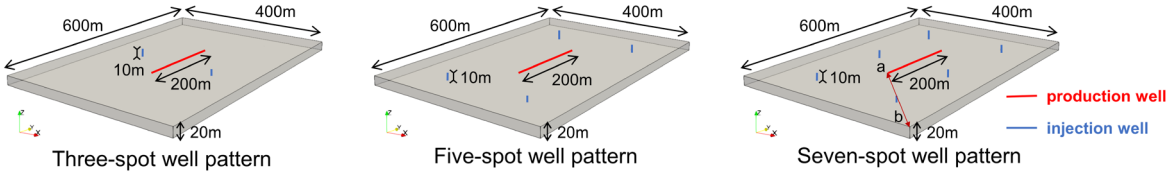

Figure 1. Schematic of multi-well water flooding models. (Blue lines and red lines represent injection wells and production wells respectively and Line ab is used for measurement of variables.)

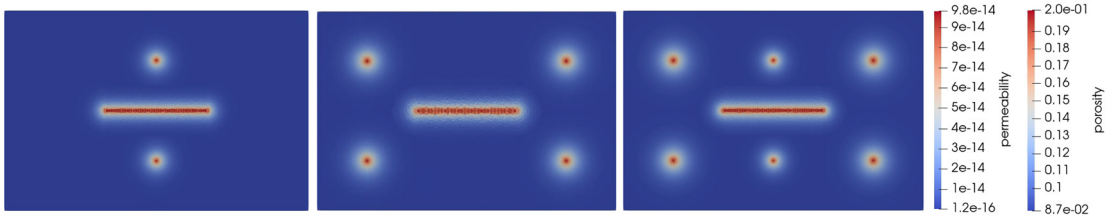

Figure 2. Exponential distribution of permeability and porosity for multi-well patterns.

Table 1. Physical properties of water, oil and rock.

Properties	Unit	Value
Young's modulus	[GPa]	30
Poisson's ratio	[\]	0.25
Biot coefficient	[\]	0.59
Thermal conductivity of oil and water	[W/(m • K)]	0.15, 0.64
Density of rock, oil and water	[kg/m^3]	2470, 800, 1000
Thermal expansivity of rock	[K^{-1}]	1.4e-5

2.3 *Modelling results*

A total of four numerical cases are simulated under either isothermal or non-isothermal conditions. Case 1 is isothermal with five-spot well pattern. The temperature difference between the initial

reservoir and the injected water is 50 ℃ in Case 2. Maintaining this temperature difference, three-spot well pattern and seven-spot well pattern are applied in Case 3 and Case 4, respectively.

From the pore pressure distribution in Figure 3, production performs better in Case 2, compared with Case 1, as the producing pressure has a wider diffusion around the production well. Compared to the isothermal condition, thermal effect decreases the fluid density and viscosity and promotes the flow of injected water so that the overall pore pressure in the reservoir is reduced, with only a slight concentration around the injection wells. In Case 3, with the three-spot well pattern less energy enhancement in the computing domain and the two injection wells are located closer to the production well. Therefore, pore pressure is lower in both the whole reservoir and around the injection wells. Pore pressure distribution under seven-spot well pattern in Case 4 integrates the results of Case 2 and Case 3 and the increased permeability in the yellow dashed circles (as shown in Figure 3) further causes a lower pressure to promote the diffusion of producing pressure.

Figure 4 compares the distribution of water-saturation in four numerical cases. Under isothermal condition, a relatively sharper saturation front is restricted obviously from the injection point to the production well with a high and concentrated saturation. In Case 2 the saturation front has not changed much but wider diffusion area around the injection well can be obtained due to lower fluid density and viscosity. A closer distance between injection and production wells in Case 3 facilitates smooth diffusion of injected water so that the saturation front is approximately semicircular. While in Case 4, the four injection wells on the left and right promotes the saturation contour in the middle two wells to spread more towards the production well.

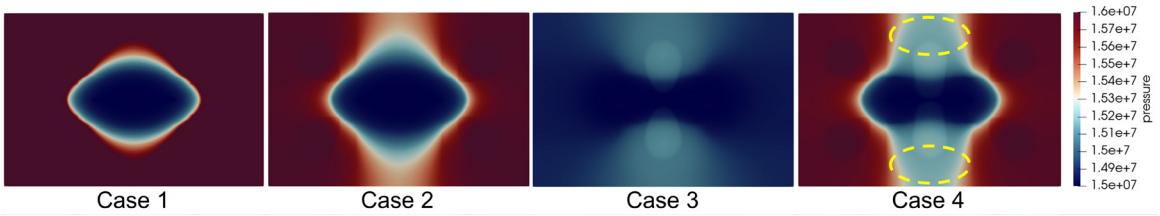

Figure 3. Pressure distribution of four numerical cases.

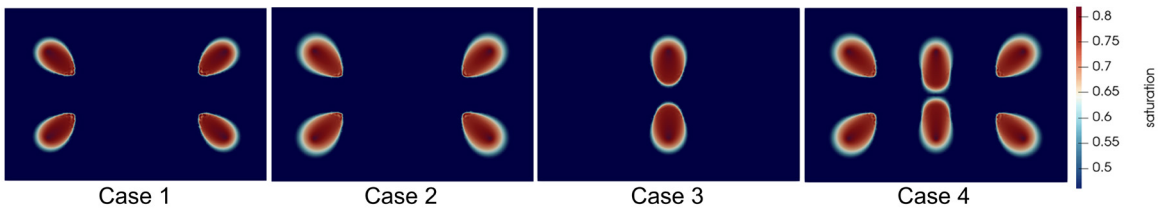

Figure 4. Saturation distribution of four numerical cases.

The influence of thermal effect on the effective stress field is investigated in Figure 5. Since there exists no induced fracture propagation, the shear stress is so small as to be negligible relative to the initial effective stress. Therefore, we still investigate the thermal stress through the stress evolution in the direction of the initial effective stress, i.e., the x direction and the y direction. Without considering injection temperature difference, the effective stress changes very slightly in both directions in Case 1 and only the production brings a stress reduction in the center. For non-isothermal cases, significant effective normal stress reduction is a consequence of the rock thermal contraction as it roughly follows the cooled down area. A temperature decrease of 50 ℃ can reduce normal effective stress about 15 MPa. If the reservoir temperature becomes higher under the influence of geothermy or other factors, the intensified thermal effect is likely to cause tensile stress, resulting in possible failure of rock near the wellbore.

Figure 6 presents the temperature and saturation variation of Case 2 along the Line ab. As shown in Figure 1, Line ab connects the production well to the corner of the model and passes through the injection well. Heat advection and conduction are very rapid in the reservoir with an obvious temperature reduction around the injection well after just one month of injection in Figure 6(a). While water diffusion is slower according to Figure 6(b). Significant water-saturation changes along the

Line ab occur after an injection interval of more than one year. Moreover, as the long-term injection proceeds, saturation front becomes fluctuant with an increase in the blue dashed circle in Figure 6(b), which represents the end of the diffusion area of saturation. This is caused by the concentration area of pore pressure around the injection well in Figure 3 which basically coincides with the diffusion area of saturation in Figure 4. The increase of pore pressure will decrease the capillary pressure and cause a higher water-saturation according to van Genuchten model.

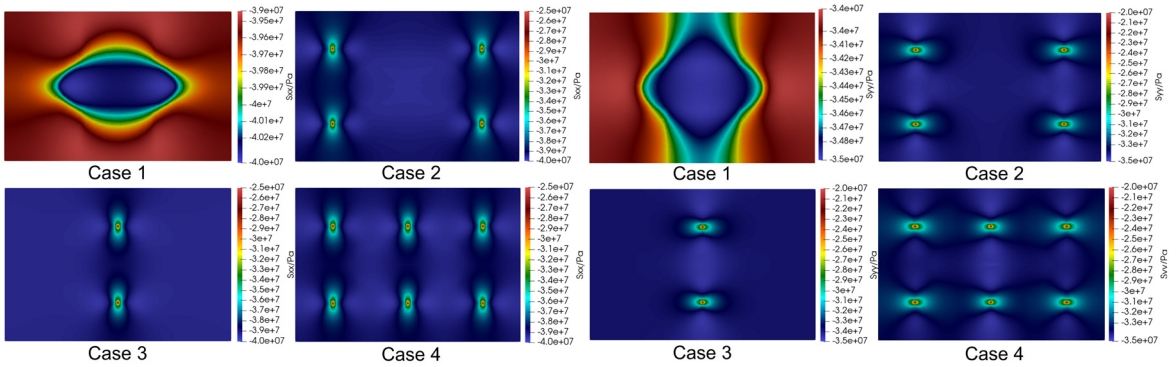

Figure 5. Effective stress distribution of 4 numerical cases.

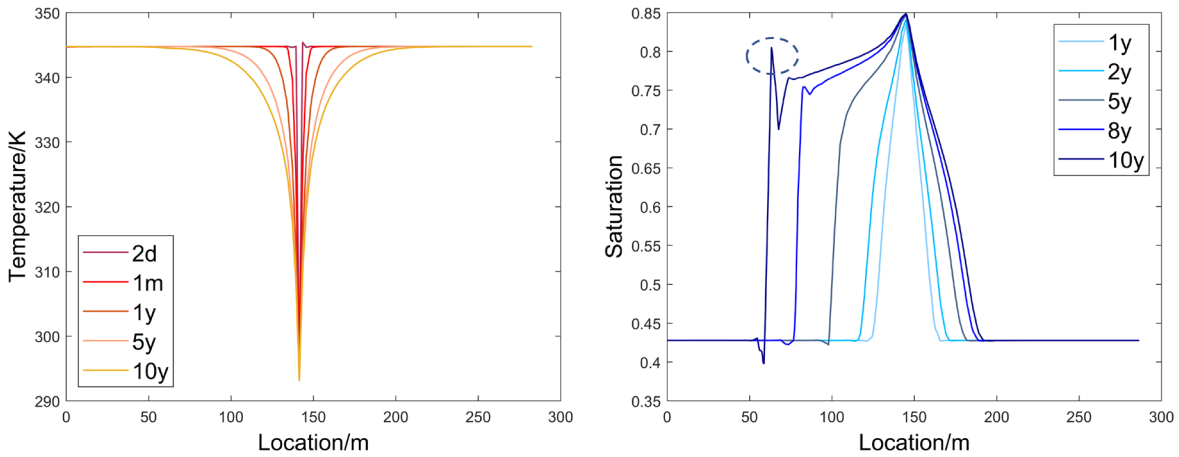

Figure 6. (a) Temperature variation between the two injection wells and (b) water-saturation between injection well and production well with different exploitation time.

3 CONCLUSIONS

An engineering-scale numerical THM modeling of long-term multi-well water flooding integrated with two phase flow is proposed. Four cases containing isothermal and non-isothermal conditions simulated the geomechanical responses in the reservoir during the injection process of cold water. Numerical results are analyzed and discussed through comparison to demonstrate the influence of thermal effect on fluid flow, effective stress and pore pressure evolution in the reservoir. It proves that high temperature caused by large buried depth will promote fluid flow to make a widen increase of saturation while decrease the effective stress to cause a possible failure of rock. Under different well patterns, spatial variation of the geomechanical variables will change but the features of evolution remain the same. The given cases provide a useful reference of engineering-scale water flooding under large reservoir depth and high temperature.

ACKNOWLEDGEMENTS

This research is funded by the National Natural Science Foundation of China (42077247) and the Fundamental Research Funds for the Central Universities.

REFERENCES

Akai, T., Blunt, M. J., & Bijeljic, B. 2020. Pore-scale numerical simulation of low salinity water flooding using the lattice Boltzmann method. *Journal of Colloid and Interface Science*, *566*, 444–453. https://doi.org/10.1016/J.JCIS.2020.01.065

Brouwer, D. R., & Jansen, J. D. 2002. *Dynamic Optimization of Water Flooding with Smart Wells Using Optimal Control Theory*. https://doi.org/10.2118/78278-ms

Douglas, Jr., J., Furtado, F., & Pereira, F. 1997. On the numerical simulation of waterflooding of heterogeneous petroleum reservoirs. *Computational Geosciences 1997 1:2*, *1*(2), 155–190. https://doi.org/10.1023/A:1011565228179

Genuchten, M. T. van. 1980. A Closed-form Equation for Predicting the Hydraulic Conductivity of Unsaturated Soils. *Soil Science Society of America Journal*, *44*(5), 892–898. https://doi.org/10.2136/SSSAJ1980.03615995004400050002X

Kolditz, O., Bauer, S., Bilke, L., Böttcher, N., Delfs, J. O., Fischer, T., Görke, U. J., Kalbacher, T., Kosakowski, G., McDermott, C. I., Park, C. H., Radu, F., Rink, K., Shao, H., Shao, H. B., Sun, F., Sun, Y. Y., Singh, A. K., Taron, J., … Zehner, B. 2012. OpenGeoSys: An open-source initiative for numerical simulation of thermo-hydro-mechanical/chemical (THM/C) processes in porous media. *Environmental Earth Sciences*, *67*(2), 589–599. https://doi.org/10.1007/S12665-012-1546-X/FIGURES/12

Magri, F., Cacace, M., Fischer, T., Kolditz, O., Wang, W., & Watanabe, N. 2017. Thermal convection of viscous fluids in a faulted system: 3D benchmark for numerical codes. *Energy Procedia*, *125*, 310–317. https://doi.org/10.1016/J.EGYPRO.2017.08.204

Parisio, F., Vilarrasa, V., Wang, W., Kolditz, O., & Nagel, T. 2019. The risks of long-term re-injection in supercritical geothermal systems. *Nature Communications*, *10*(1). https://doi.org/10.1038/s41467-019-12146-0

Patel, H. V., Das, S., Kuipers, J. A. M., & Peters, E. A. J. F. 2019. Direct numerical simulations of water flooding process through digitized porous rocks. *Chemical Engineering Science: X*, *4*, 100041. https://doi.org/10.1016/J.CESX.2019.100041

Xu, W. J., Shao, H., Hesser, J., Wang, W., Schuster, K., & Kolditz, O. 2013. Coupled multiphase flow and elasto-plastic modelling of in-situ gas injection experiments in saturated claystone (Mont Terri Rock Laboratory). *Engineering Geology*, *157*, 55–68. https://doi.org/10.1016/J.ENGGEO.2013.02.005

Zhai, L., Yang, M., Yan, C., Tian, T., & Huang, S. 2022. Dynamic Distribution Characteristics of Oil and Water during Water Flooding in a Fishbone Well with Different Branch Angles. *ACS Omega*, *7*(31), 27206–27215. https://doi.org/10.1021/ACSOMEGA.2C01918

Zhang, L., Dou, H., Wang, T., Wang, H., Peng, Y., Zhang, J., Liu, Z., Mi, L., & Jiang, L. 2022. A production prediction method of single well in water flooding oilfield based on integrated temporal convolutional network model. *Petroleum Exploration and Development*, *49*(5), 1150–1160. https://doi.org/10.1016/S1876-3804(22)60339-2

Zhang, R. han, Zhang, L. hui, Luo, J. xin, Yang, Z. dong, & Xu, M. yang. 2016. Numerical simulation of water flooding in natural fractured reservoirs based on control volume finite element method. *Journal of Petroleum Science and Engineering*, *146*, 1211–1225. https://doi.org/10.1016/J.PETROL.2016.08.024

Zheng, S., Hwang, J., Manchanda, R., & Sharma, M. M. 2021. An integrated model for non-isothermal multi-phase flow, geomechanics and fracture propagation. *Journal of Petroleum Science and Engineering*, *196*, 107716. https://doi.org/10.1016/J.PETROL.2020.107716